Synthetic waveforms of axial motion in a borehole with drill string

Biancamaria Farina,[a] Flavio Poletto, and José M. Carcione
Istituto Nazionale di Oceanografia e di Geofisica Sperimentale–OGS, Borgo Grotta Gigante 42/c, 34010 Sgonico, Trieste, Italy

(Received 13 October 2015; revised 29 July 2016; accepted 19 January 2017; published online 15 February 2017)

This work studies the wave motion in a fluid-filled borehole in the presence of drill string and geological formation. The synthetic waveforms are obtained by a three-dimensional axis-symmetric full-wave numerical simulation in a two-dimensional multi-domain where the medium is uniform with respect to the azimuth. The discretization is performed in cylindrical coordinates. In order to simulate the waves at the origin (axis of the polar radius), a very small radius is used to avoid the singularity. The free-surface and rigid boundary conditions are tested and it is shown that the rigid one constitutes the best approximation. The simulations provide the amplitude distribution and motion diagrams in the borehole vertical cross-sections and at the outer boundary, away from the borehole. Propagation in the presence of hard and soft formations is analysed. The dispersion, the amplitude, and the orbital polarization of the modes excited by a point source acting in the fluid inside a drillstring are considered and examples of comparison with literature results obtained using multi-modal analysis are shown. The proposed approach is more general than the multi-modal analysis, since it allows for arbitrary variations of the properties in the plane of symmetry.
 [http://dx.doi.org/10.1121/1.4976043]

[JFL] Pages: 828–839

I. INTRODUCTION

The study of acoustic wavefield propagation in fluid-filled boreholes with drilling tubulars is of great importance for many applications of downhole monitoring in oil and gas exploration, well drilling, well completion, and production surveillance (e.g., Refs. 1–6). The analysis of the recorded data involves the interpretation of the propagating wavefields, which is supported by the analysis in the low frequency approximation of the coupled wave modes in the different borehole domains including the radiation in the surrounding formation,[1,5,7,8] and full-wave numerical simulation.[9–11]

Numerical simulation is therefore a powerful tool to provide predictions and support interpretation of wavefields recorded in real conditions. When the analysis includes the propagation of acoustic signals in the formation at seismic distances from the borehole, a main issue is the different scale to simulate the wavefields in the borehole, where a radial discretisation of millimetres is typically needed, and the formation, where the propagation requires cells of tens of meters to reach distances of hundred of meters away from the borehole. Here, we restrict the analysis to distances close to the borehole wall. However, even in this case, cylindrical multi-domains and non-uniform radial rings are necessary to implement radial layers and obtain full-wave numerical solutions.[11,12]

Approaches based on analytical methods[7,8,13] provide the basis for the calculation of the multi-modal solutions in systems composed of layered cylindrical sections in fluid-filled boreholes.[14] Karpfinger *et al.*[15] propose a spectral-method algorithm to study wave propagation of acoustic modes in elastic cylindrical structures, in which the problem of determining the modal dispersion is expressed as a generalised eigenvalues problem.

Numerical algorithms implemented in cylindrical coordinates require irregular radial grids to represent with appropriate detail the physical properties of the borehole-formation system.[9,11] This approach poses the problem to properly define the boundary conditions in the axis of the borehole, which is located in the inner fluid of the drill string. If the aim of the study is to simulate phenomena associated with the borehole and the characterisation of the wavefields in the formation, the role of the inner boundary, which is masked by the presence of the pipe might not be significant. For instance, Kessler and Kossloff[10] propose a method implementing a free-surface boundary condition near the origin, using cylindrical coordinates. However, when the analysis focus on the signal in the inner mud, the choice of the inner boundary condition is important. The free-surface boundary condition zeroes the inner pressure near the radial origin. Thus the pressure field is weakened in the inner fluid domain inside the drill pipe near the origin, where it vanishes. Here, we analyse the free-surface and rigid boundary conditions and show that the rigid one preserves the mode of the innermost fluid domain. A scheme of the reflection of waves from the inner boundary in the axis-symmetric geometry is shown in Fig. 1.

II. EQUATIONS OF MOTION AND ALGORITHM

We design a two-dimensional (2-D) algorithm implemented for solving three dimensional axis-symmetric elastic

[a]Electronic mail: bfarina@inogs.it

 0001-4966/2017/141(2)/828/12/$30.00

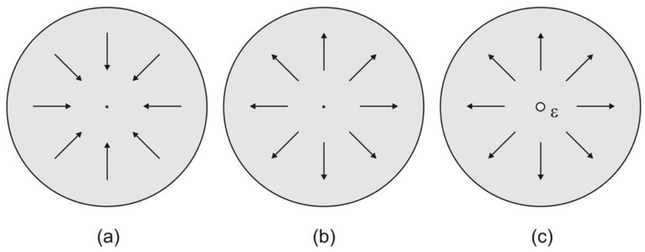

FIG. 1. Reflection of waves in the axis-symmetric geometry. (a) Inward and (b) Outward cylindrical wavefields at the origin are modeled by the rigid boundary condition, which represents (c) The reflected outcoming waves at the axis, with a negligible delay through the small inner disk portion (of radius ε) surrounded by the boundary. The sign of the inner reflection coefficient changes for pressure and velocity.

wave equation in fluid-filled boreholes in the presence of drill string.[11] The algorithm uses a multi-domain approach and the problem is solved in cylindrical coordinates r, z, and θ, representing the distance from the centre of the borehole, the depth, and the polar angle, respectively. According to the axis-symmetry, the medium is uniform with respect to the azimuth. The simulation is performed by using Chebyshev and Fourier differential operators to calculate the spatial derivatives along the radial and vertical direction, respectively, and a fourth-order Runge-Kutta time-integration scheme. The numerical technique is based on the combination of the equation of momentum conservation and stress-strain relation calculated for solid (drill pipe, casing, formation) and fluid layers (inner and outer mud).

A free surface or rigid boundary condition is applied in the innermost boundary, i.e., the axis of the borehole, while a non-reflecting boundary condition is applied in the outermost boundary, i.e., the formation external boundary. Wave modes and radiated waves are simulated in the borehole-formation system, and we show that rigid boundary is necessary to preserve the pressure component of the mode that propagates in the inner mud.

A. Equations of motion

The 2-D numerical simulation of three-dimensional (3-D) axis-symmetric seismic wave propagation is based on the solution of the equations of momentum conservation combined with the stress-strain relations. We consider the equations for solid [i.e., pipe (drill string), casing and formation] and fluid (inner and outer mud) layers. The equations of momentum conservation, expressed in cylindrical coordinates (r, z, θ), for the solid are[11,12]

$$\rho\dot{v}_r = \frac{\partial\sigma_{rr}}{\partial r} + \frac{\partial\sigma_{rz}}{\partial z} + \frac{1}{r}(\sigma_{rr} - \sigma_{\theta\theta}) + f_r, \tag{1}$$

$$\rho\dot{v}_z = \frac{\partial\sigma_{rz}}{\partial r} + \frac{\partial\sigma_{zz}}{\partial z} + \frac{\sigma_{zr}}{r} + f_z, \tag{2}$$

where v, σ, and ρ represent particle velocity, stress, and mass density, respectively, and f_r and f_z are excitation body forces per unit volume. A dot above a variable denotes time differentiation. The equations of momentum conservation for the fluid are

$$\rho\dot{v}_r = \frac{\partial\sigma_{rr}}{\partial r}, \quad \rho\dot{v}_z = \frac{\partial\sigma_{rr}}{\partial r}, \tag{3}$$

where $-\sigma_{rr}$ is the fluid pressure.

The stress-strain relations in cylindrical coordinates for the solid are

$$\dot{\sigma}_{rr} = (\lambda + 2\mu)\frac{\partial v_r}{\partial r} + \lambda\left(\frac{\partial v_z}{\partial z} + \frac{v_r}{r}\right), \tag{4}$$

$$\dot{\sigma}_{\theta\theta} = \lambda\left(\frac{\partial v_r}{\partial r} + \frac{\partial v_z}{\partial z}\right)\frac{\partial v_r}{\partial r} + (\lambda + 2\mu)\frac{v_r}{r}, \tag{5}$$

$$\dot{\sigma}_{zz} = (\lambda + 2\mu)\frac{\partial v_z}{\partial z} + \lambda\left(\frac{\partial v_r}{\partial r} + \frac{v_r}{r}\right), \tag{6}$$

$$\dot{\sigma}_{rz} = \mu\left(\frac{\partial v_r}{\partial z} + \frac{\partial v_z}{\partial r}\right), \tag{7}$$

where λ and μ are the Lamé constants. The stress-strain relation of the fluid is

$$\dot{\sigma}_{zz} = \lambda\left(\frac{\partial v_r}{\partial r} + \frac{\partial v_z}{\partial z} + \frac{v_r}{r}\right) + \dot{f}_{rr}, \tag{8}$$

where f_{rr} is a dilatational source per unit volume.

B. Solution scheme and boundary conditions

The equations of motion contain both spatial and temporal derivatives. The numerical solution is achieved by using the Chebyshev and the Fourier expansion to calculate the spatial derivatives along the radial and the vertical direction, respectively, and the fourth order of the Runge-Kutta scheme to perform the time integration.

The domain is decomposed in four (or more) subdomains corresponding, in principle, to the inner mud, drill string, outer mud, and casing/formation media. Each subdomain is non-uniformly discretized with the Gauss–Lobatto collocation points along the radial direction and uniformly discretized along the vertical direction.[11] To combine two adjacent meshes, the wavefield is decomposed in incoming and outgoing wave mode at the interfaces between the media and these modes are modified on the basis of the fluid/solid boundary conditions[12] (Chaps. 9.3.2 and 9.5). The ingoing waves are connected with the solution outside the subdomains and are calculated by the boundary condition of stress- and particle velocity-components continuity. The outcoming waves, instead, depend on the solution inside the subdomains (e.g., Refs. 9, 16, and 17). The connection of two grids at their common boundary is carried out by adopting the characteristic variables of the wave equation.[9,11,18]

To model the singularity at the borehole axis ($r = 0$), the minimum radius ($r = \varepsilon$) of the innermost mesh has been taken different from zero but small with respect to the wavelength. Free surface or rigid body boundary conditions are applied at the inner radius boundary of the innermost mesh ($r = \varepsilon$, Fig. 2), while a non-reflecting boundary condition is applied at the outer radius of the outermost mesh ($r = d$, Fig. 2), by appropriately setting the characteristic variables.[9,11,18]

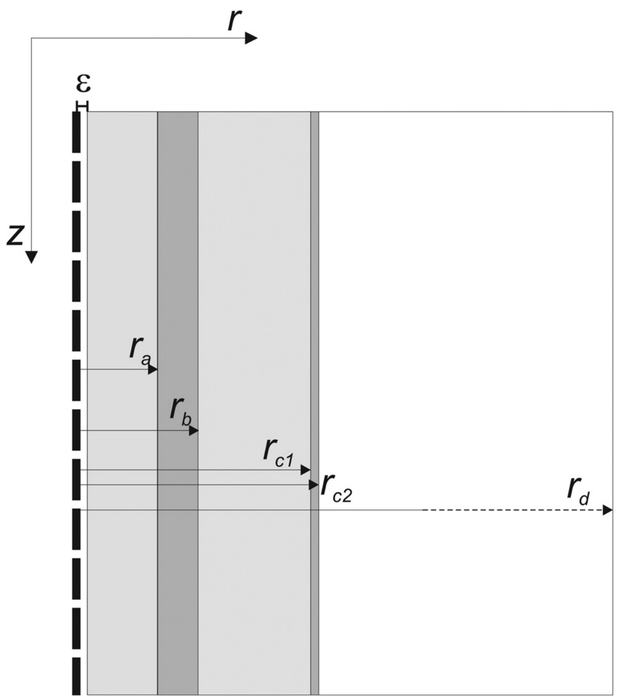

FIG. 2. Section of the borehole-pipe-formation system, modified after Carcione *et al.* (Ref. 11). The ranges of each mesh are $r_a - \varepsilon$ for the inner mud, $r_b - r_a$ for the drill pipe, $r_{c_1} - r_b$ for the outer mud, $r_{c_2} - r_{c_1}$ for the casing and $r_d - r_{c_2}$ for the formation. The dashed line represents the borehole axes.

Carcione *et al.*[11] showed results obtained with the application of the free-surface boundary condition at the innermost boundary. They presented the comparison between numerical and analytical solutions, with a reciprocity test, simulation of the propagating modes and analysis of propagation velocities. The free-surface boundary condition of zero traction (pressure in fluid) does not preserve the pressure mode component at $r = \varepsilon$ (Fig. 2). Therefore, among different boundary conditions,[9,11] in order to model the wave motion in the drill string mud channel we choose the rigid condition at the innermost boundary. This condition is achieved by retaining the characteristic variable that describes inward motion and zeros the radial particle velocity. The resulting relations are[19]

$$v_r^{(n)} = 0 \tag{9}$$

and

$$\sigma_{rr}^{(n)} = \sigma_{rr}^{(o)} - \rho V_p v_r^{(o)}, \tag{10}$$

where the superscripts "*o*" and "*n*" denote old and new values of variables before and after the application of the boundary condition, respectively.

III. NUMERICAL SIMULATIONS

A. Comparison between analytical and numerical solutions

To test the algorithm and verify the performance of the rigid boundary condition at the origin we compare numerical and analytical solutions for acoustic axis-symmetric propagation in two cases.

The first example considers a homogeneous fluid with compressional velocity $V_P = 1558$ m/s and density $\rho = 1000$ kg/m^3. We show in Fig. 3 the model and the pressure signals, recorded in two different radial points, corresponding to the analytical solution (solid line) and numerical simulation (dotted line). To obtain the analytical solution we consider a ring source, with radius $R_c = 16$ m, composed of 10 000 point sources. The analytical signal at the receiver is the linear superposition of the Green functions of all the point sources.[11] The numerical simulation uses one mesh with radial and vertical dimensions of 74 and 200 m, discretized with 91 and 250 grid points, respectively. The innermost radius is $r = \varepsilon = 1$ cm, where the rigid boundary condition is applied [Eqs. (9) and (10)]. Both in the analytical and numerical simulations the point source is a Ricker wavelet with a pick frequency of 250 Hz. The solutions of the pressure signal are acquired at $R = 3$ cm [Fig. 3(a)] and $R = 16$ m [Fig. 3(b)] from the borehole axis (and from the source-ring center). The bold dotted and the dotted arrows show the ray paths from the source to the receivers for the analytical and numerical simulations, respectively. The first arrivals present the same phases since the signal paths for both solutions are the same [ray paths 1 in Figs. 3(a) and 3(b)]. The phases of the second arrival are opposite because in the numerical case the signal is reflected by the innermost boundary, while in the analytical case it arrives from the farthest sources [ray path 2 in Fig. 3(b)]. The agreement is good and the presence of the rigid boundary

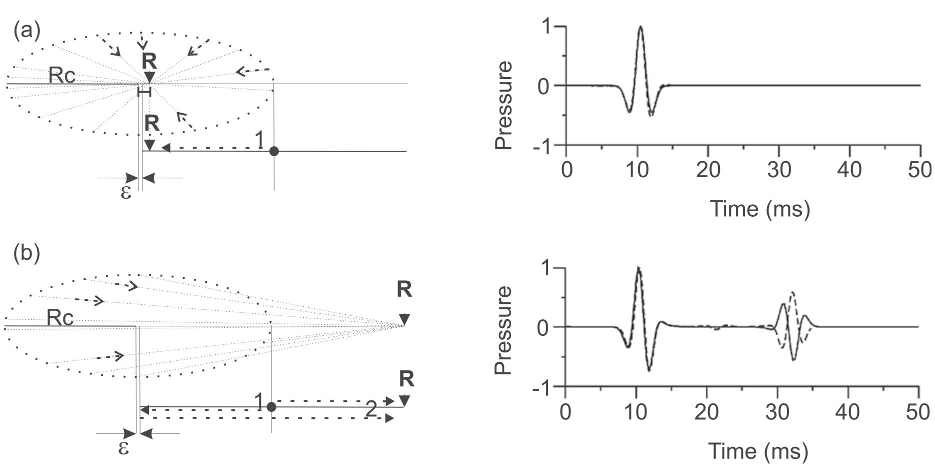

FIG. 3. Model and comparison between the analytical (solid line) and numerical (dotted line) signals recorded by (a) a receiver located at 3 cm from the borehole axis and (b) a receiver located at 16 m from the borehole axis. The numerical signals are obtained by using the rigid boundary condition in the innermost domain [figure modified after Carcione *et al.* (Ref. 11)].

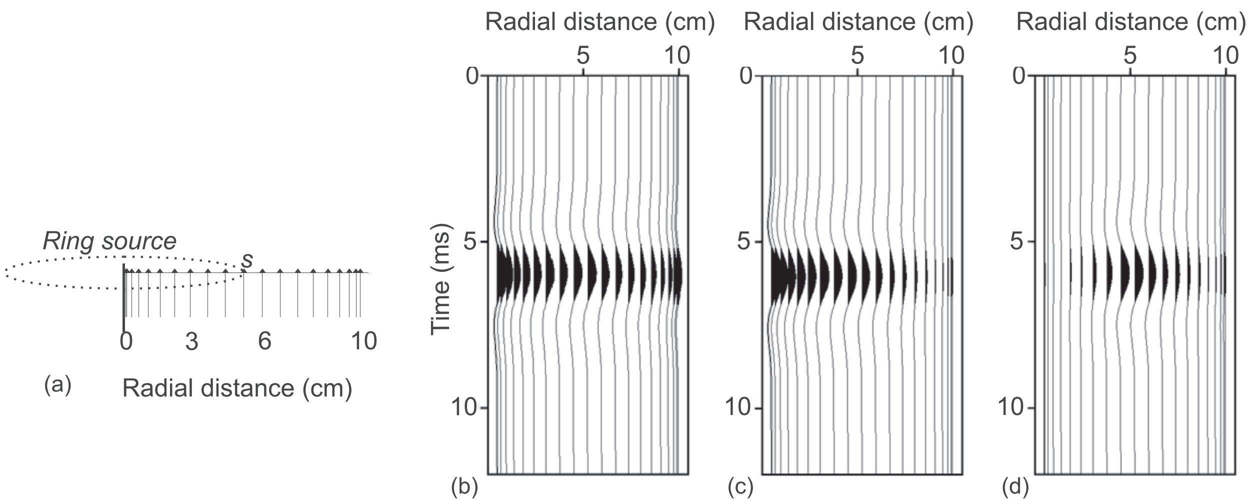

FIG. 4. Model used to obtain the analytical solution and numerical simulation (a). The triangles shows the receiver radial position. (b) Analytical pressure signals compared with the numerical pressure signals calculated using the rigid (c), and free-surface (d) boundary conditions.

implies a non-zero signal pressure near the borehole discontinuity whereas, by definition, the free-surface condition implies zero σ_{rr}.

The second example consists in a smaller mesh of homogeneous fluid with compressional velocity $V_P = 1304$ m/s and density $\rho = 1500\,\mathrm{kg/m^3}$. The numerical domain, 125 m depth, is radially discretized with 21 Gauss–Lobatto collocation points [black lines in Fig. 4(a)]. The outermost radius is 10 cm and the innermost one (ε) is 0.5 cm. The dilatational source (S) is located at 5.25 cm from the borehole axis. The radius of the ring source made of 1000 point sources to obtain the analytical simulation, is 5.25 cm. Figures 4(b), 4(c), and 4(d) show the pressure signals for the analytical solution and numerical simulations with rigid and free-surface boundary, respectively. The signals at the outermost boundary (numerical simulation) vanish due to the presence of absorbing boundaries. The signals at the innermost boundary, near the borehole discontinuity vanishes only when the free-surface boundary is applied, while the rigid boundary preserves the signal pressure near the borehole axis and the comparison with the analytical result shows a good agreement. A detail of the pressure component as a function of the radial distance from the borehole discontinuity to the source is shown in Fig. 5. The analytical result (ANA) is compared with the numerical simulation calculated by using the rigid boundary condition [NRB in Fig. 5(a)] and free surface boundary conditions [NFS in Fig. 5(b)] and the differences (DIF) are shown for both cases. It can be observed how the rigid boundary condition performs better at the borehole discontinuity.

B. Simulation of propagation modes

Next, using the rigid body boundary condition, we simulate wave propagation in a fluid-filled borehole with a drill string considering two different formations surrounding the well, namely, a hard formation, where the shear velocity is higher than the fluid acoustic velocity, and a soft formation, where the shear velocity is lower than the fluid velocity. The material and geometrical properties of the models are the same of that of Lea and Killingstad[8] and are reported in Table I. The inner mud, drill pipe, and outer mud are radially discretized with $n_r = 11$ grid points, while the formation is radially discretized with $n_r = 91$ grid points. The 160 m depth interval is discretized with 300 grid points equally

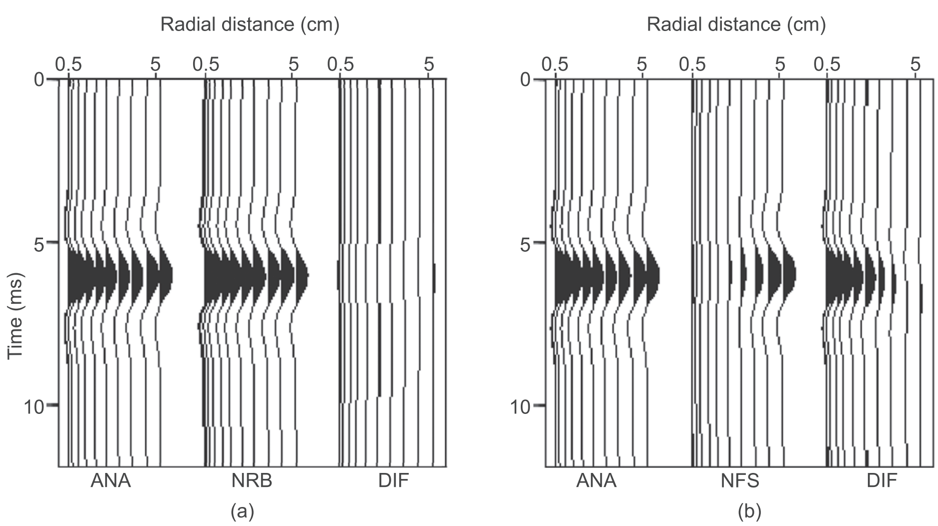

FIG. 5. Detail of the pressure component from the borehole discontinuity to the source location for the example shown in Fig. 4. (a) Analytic solution (ANA), numerical simulation with rigid boundary (NRB), and the difference (DIF). (b) Analytic solution (ANA), numerical solution with free surface boundary (NFS), and the difference (DIF).

TABLE I. Material and geometrical properties.

	v_P (m/s)	v_S (m/s)	ρ (g/cm^3)	ε (cm)	r_a (cm)	r_b (cm)	r_c (cm)	r_d (m)
Inner mud	1304	0	1.000	0.27	5.4	—	—	—
Drill pipe	5943	3177	7.850	—	5.4	6.35	—	—
Outer mud	1304	0	1.000	—	—	6.35	17.0	—
Hard formation	3290	1900	2.000	—	—	—	17.0	20
Soft formation	1423	822	2.000	—	—	—	17.0	20

spaced with $\Delta z = 53.6$ cm. The perturbation is a dilatational source applied in the center of the inner fluid at a depth of 128 m. The source is a Ricker wavelet with peak frequency 375 Hz and time duration of 12 ms. The solution is propagated up to 70 ms with a time step of 10 ns and the output time traces are resampled to 10 μs. We record pressure and vertical and radial particle-velocity components in the vertical and radial directions of all the subdomains (a vertical array at a fixed radial position provides a vertical seismic profile or VSP).

We observe the three propagating borehole modes (associated to the inner mud, drill pipe, and outer mud) expected in the low frequency solutions for a frequency below 1 kHz,[1] which are generated by the radial motion of the drill string and formation that allows the pressure waves inside the string to communicate with the annulus.

The inner fluid mode, denoted by M1, is characterized by a dominant motion in the inner mud and determined

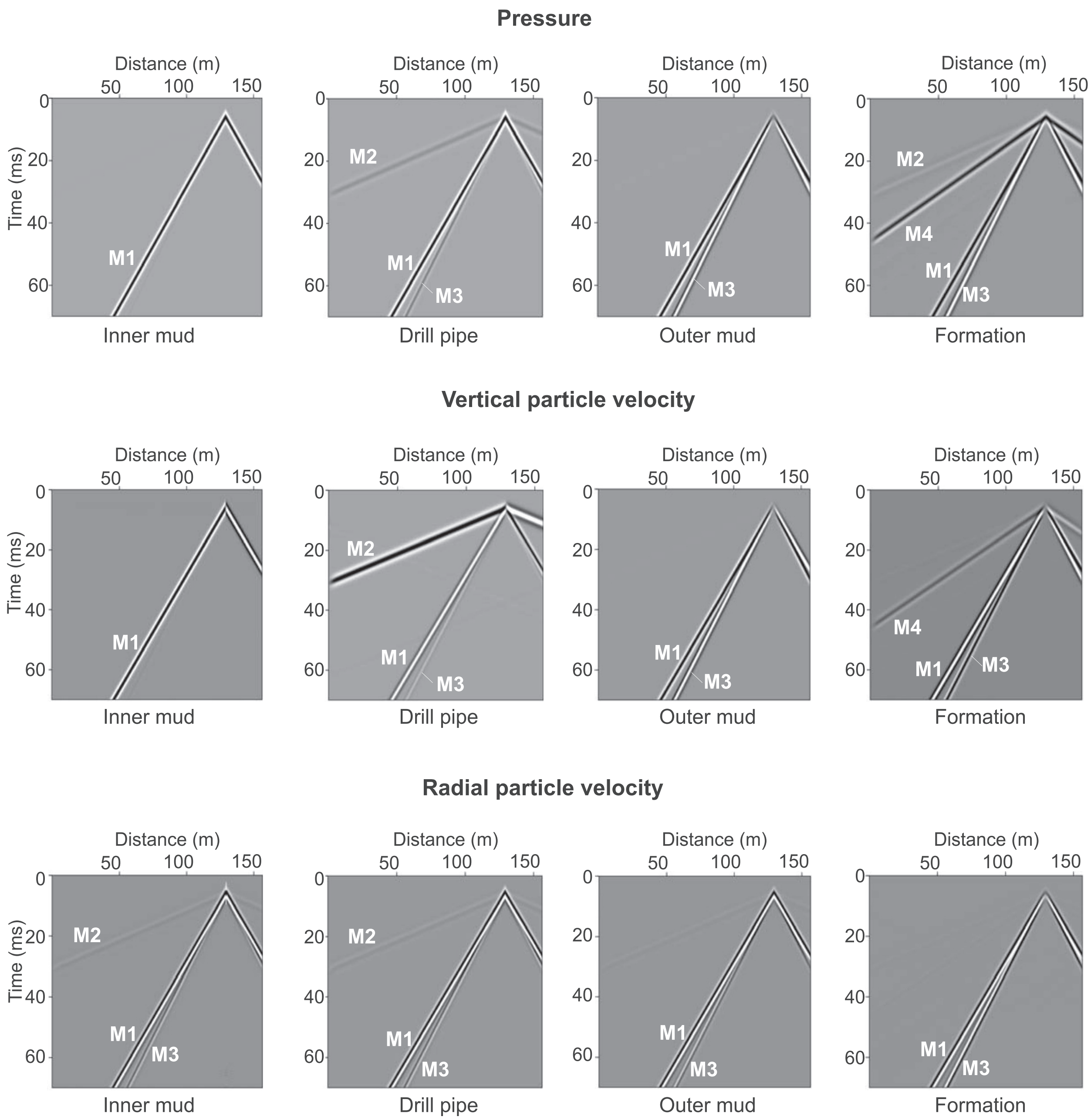

FIG. 6. Hard formation. VSP of pressure, vertical and radial particle velocity wavefields recorded at the center of the inner mud, drill pipe, outer mud and formation with a receiver located at 1 m from the outer mud/formation interface. The labels indicate the modes: M1 (inner mud mode), M2 (drill string mode), M3 (outer mud mode), and M4 (formation mode).

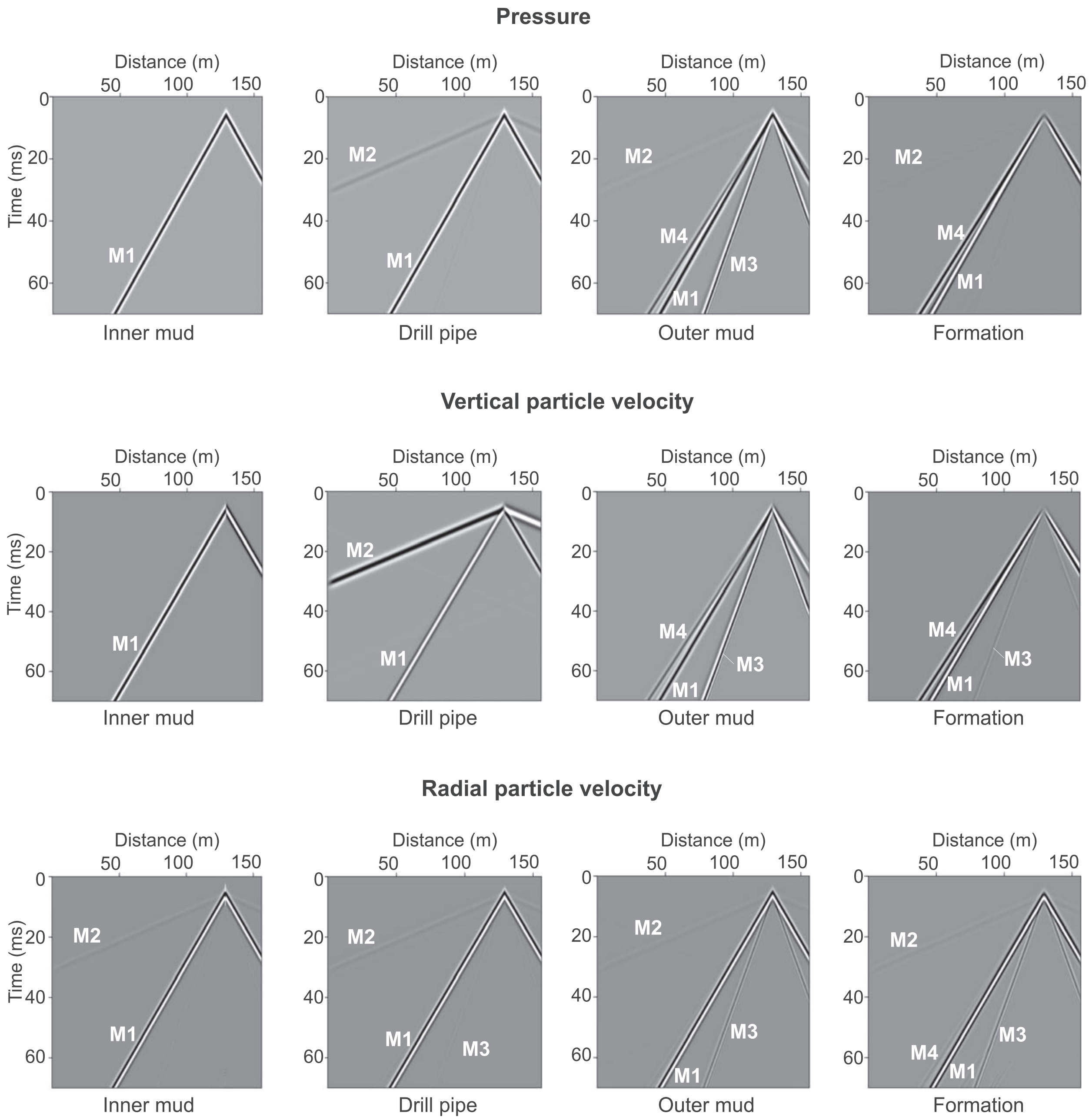

FIG. 7. Soft formation. VSP of pressure, vertical, and radial particle velocity wavefields recorded at the center of the inner mud, drill pipe, outer mud, and formation with a receiver located at 1 m from the outer mud/formation interface. The labels indicate the modes: M1 (inner mud mode), M2 (drill string mode), M3 (outer mud mode), and M4 (formation mode).

mainly by the properties of the inner mud and drill pipe. The mode M2 (drill pipe mode) that has motion and stress mainly over the cross-section of the pipe,[1] represents the extensional wave traveling in the drill string. The mode M3 (outer fluid mode) is strongly influenced by the formation and weakly by the pipe. We observe also another mode characterized by dominant motion in the formation, that we call M4, which is significantly influenced by the compressional wave propagating in the formation.

Figures 6 and 7 show the VSP of pressure, vertical and radial particle velocity fields recorded in the center of the inner mud, drill pipe, outer mud, and formation at a radial distance 1 m from the outer mud/formation interface, for the hard and the soft formation, respectively. In each subdomain,

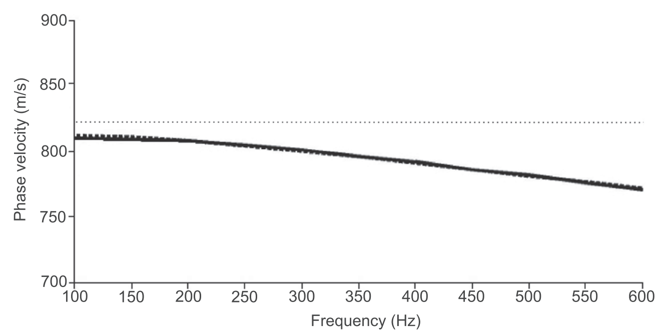

FIG. 8. Dispersion characteristic of mode M3 in the presence of a soft formation calculated with the free-surface (dotted bold line) and rigid (solid bold line) boundary conditions. The dotted line represents the formation shear-wave velocity.

TABLE II. Material and geometrical properties. Soft formation with drill collar (Ref. 1).

	v_P (m/s)	v_S (m/s)	ρ (g/cm^3)	ε (cm)	r_a (cm)	r_b (cm)	r_c (cm)	r_d (m)
Inner mud	1558	0	1.000	0.19	3.81	—	—	—
Drill collar	5900	3400	7.800	—	3.81	10.16	—	—
Outer mud	1558	0	1.000	—	—	10.16	15.24	—
Soft formation	1409	813	2.000	—	—	—	15.24	100

the modes are interpreted and highlighted. The presence of a rigid boundary condition allows us to observe the inner fluid mode M1, which is not detectable using the free surface boundary condition. We calculate the mode velocities by picking the arrival time at the maximum of its energy and analyze the travel times as a function of depth.

Mode M2 is the dominant mode in the drill string and the measured velocity is 5142 and 5137 m/s with the hard and soft formation, respectively, in agreement with Rama Rao and Vandiver[1] who measured a velocity slightly faster in the hard formation compared to that of the soft formation. Mode M1 is dominant in the inner fluid and its velocity is 1290 and 1286 m/s in the hard and soft formation, respectively. Modes M1 and M2 are weakly influenced by the variations in the formation properties and are non-dispersive. Mode M3, which is dominant in the outer mud, is strongly affected by formation properties. In the hard formation, this mode is weakly dispersive and its velocity slightly increases with frequency, as shown by Rama Rao;[13] it varies from 1110 and 1119 at 100 and 600 Hz, respectively. On the other hand, in the soft formation mode M3 is strongly dispersive and its phase velocity decreases as the frequency increases.[13]

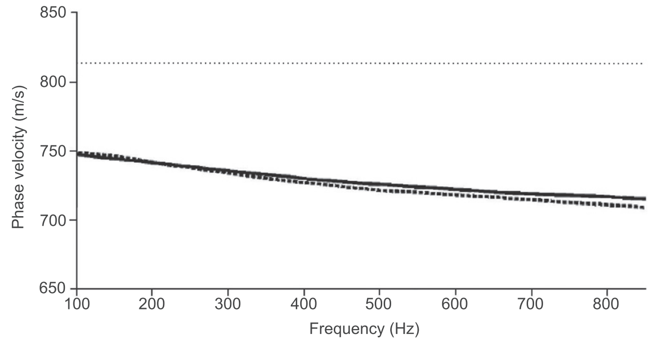

FIG. 9. Mode M3 dispersion curves corresponding to the numerical simulation (solid line) and analytical solution (dotted line) using the properties listed in Table II.

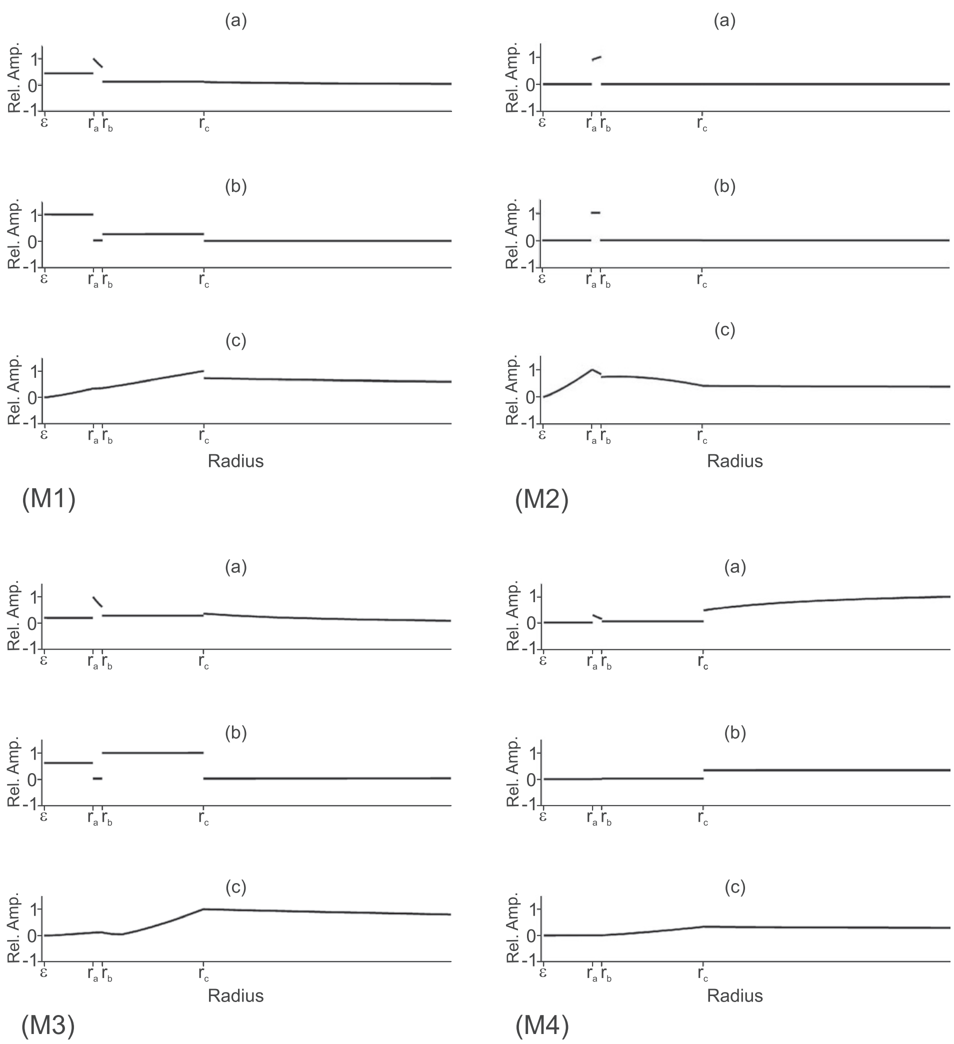

FIG. 10. Hard formation. Amplitude analysis of pressure (a), vertical (b), and radial (c) particle velocity components for modes M1, M2, M3, and M4. RMS amplitudes are represented as a function of the radial distance (ε is the innermost radius, r_a, r_b, and r_c are the inner-mud, drill-pipe, and outer-mud radii, respectively).

The measured phase velocity changes from 810 to 771 m/s, when the frequency goes from 100 to 600 Hz.

In the range of investigated frequencies, using the geometric and physical properties given in Table I, mode M3 radiates energy into the soft formation, while its energy is trapped within the borehole in the hard formation. Mode M4 has a velocity of 3210 and 1416 m/s for the hard and soft formation, respectively, close to the two formation compressional velocities.

To test the velocity variations with respect to the boundary conditions applied in the innermost domain, we simulate wave propagation with the soft formation using the free-surface and rigid boundary conditions. Using the first condition, which zeros the stress at the discontinuity, the weakened inner mud mode M1 is not detectable, therefore we compare the velocity of modes M2, M3, and M4.

The pipe mode speeds M1 are 5137 and 5130 m/s with the rigid and free-surface conditions, respectively, while the velocities of the formation mode are 1416 and 1415 m/s, respectively. Since the outer mud mode M3, in the presence of the soft formation, is dispersive, we show the dispersion curves calculated with the two conditions in Fig. 8. We observe that the velocity variation is weakly sensitive to the condition type used in the inner domain. The effect induced by the boundary condition creates small fluctuations in the mode velocities.

For comparison, we calculate the mode M3 dispersion curve in the presence of soft formation using the analytical approach proposed by Rama Rao and Vandiver[1] with a model using the properties given in Table II. We compare the results with our simulations using the rigid boundary condition that has proven to be the best choice to model all the coupled modes generated in a fluid-filled borehole surrounded by the formation. Figure 9 shows the comparison, where the solid and dotted line represents the dispersion obtained using the numerical and analytical approaches, respectively. The dashed line represents the shear-wave formation velocity. The agreement is good.

IV. SIGNAL ANALYSIS

Although the modal analysis of multi-domain guided waves identifies fundamental modes characterized by the same propagation velocity in all the domains, the amplitude of the modal vibrations varies in the domains, with different curves for the different components. We analyze amplitude and orbital polarization of the motion vibrations of the simulated signals obtained in the multi-domain using a

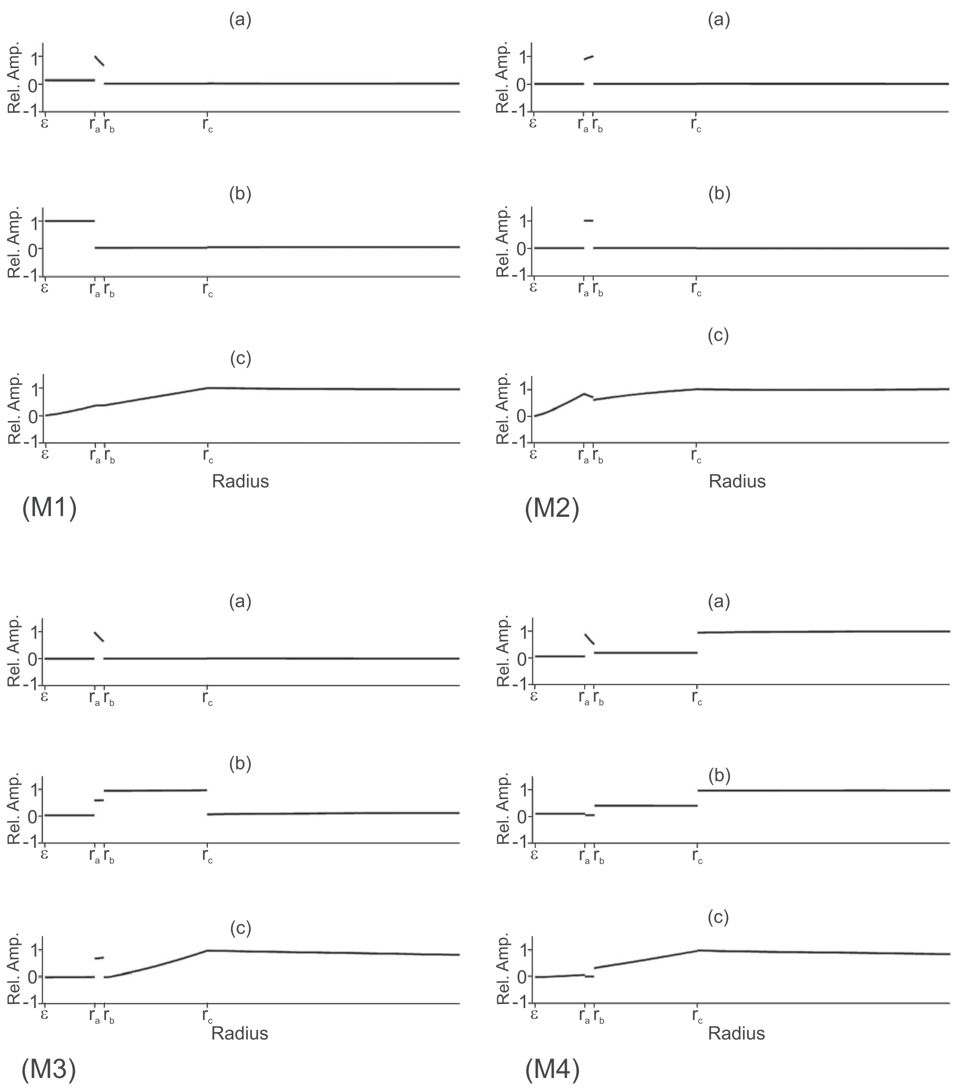

FIG. 11. Model with soft formation. Amplitude analysis of pressure (a), vertical (b), and radial (c) particle velocity components for modes M1, M2, M3, and M4. RMS amplitudes are represented as a function of the radial distance (ε is the innermost radius, r_a, r_b, and r_c are inner-mud, drill-pipe, and outer-mud radii, respectively).

dilatational source in the inner mud with applied rigid-boundary condition at hole axis, corresponding to a model defined by the properties given in Table I.

A. Amplitude

To calculate the mode amplitude, we record the VSP signals at every radial grid point of each domain and select the depth interval that better evidences the signals that we consider, paying attention to avoid local amplitude variations in near the source. At each radial position of the single domain, we align the selected mode and subsequently stack it in depth to minimize unwanted events. Then, we calculate the RMS amplitude of the stacked data and plot the normalized amplitude curves as a function of the radial distance. Figures 10 and 11 show the amplitude analysis for the hard and soft formations, respectively, for pressure (a), and the vertical (b), and radial (c) particle-velocity components of the inner mud M1, drill pipe M2, outer mud M3, and formation M4 modes. The pressure, axial, and radial particle-velocity components of the drill pipe mode M2 have a mode-shape similar in both the hard and soft formation (Figs. 10 and 11, M2). The axial particle velocity and the pressure are uniform over the cross section of the pipe, and concentrated in the pipe domain. The radial particle velocity increases in the inner fluid domain for both formations, reaching a maximum at the interface with the drill pipe where it decreases. The vertical particle-velocity component of modes M1 and M3 is uniform and concentrated in the inner and outer fluid layer, respectively, while the pressure component of these modes is dominant in the drill pipe, which is stiffer, for both formations. Mode M4 has pressure,

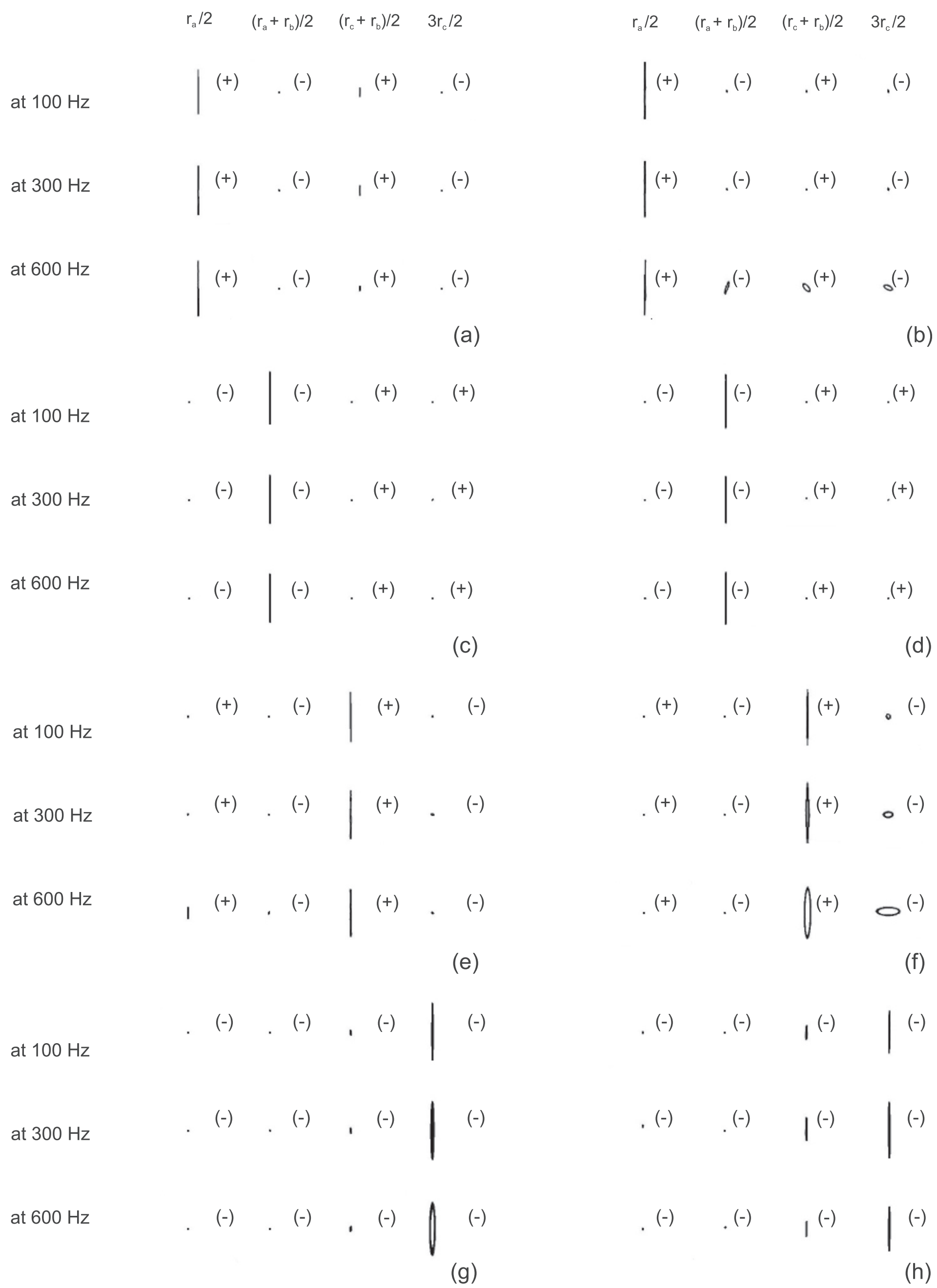

FIG. 12. Polarization in the presence of hard [(a), (c), (e), (g)] and soft [(b), (d), (f), (h)] formations of modes M1 [(a), (b)], M2 [(c), (d)], M3 [(e), (f)], and M4 [(g), (h)] at 100, 300, and 600 Hz. The model properties and dimensions are shown in Table I.

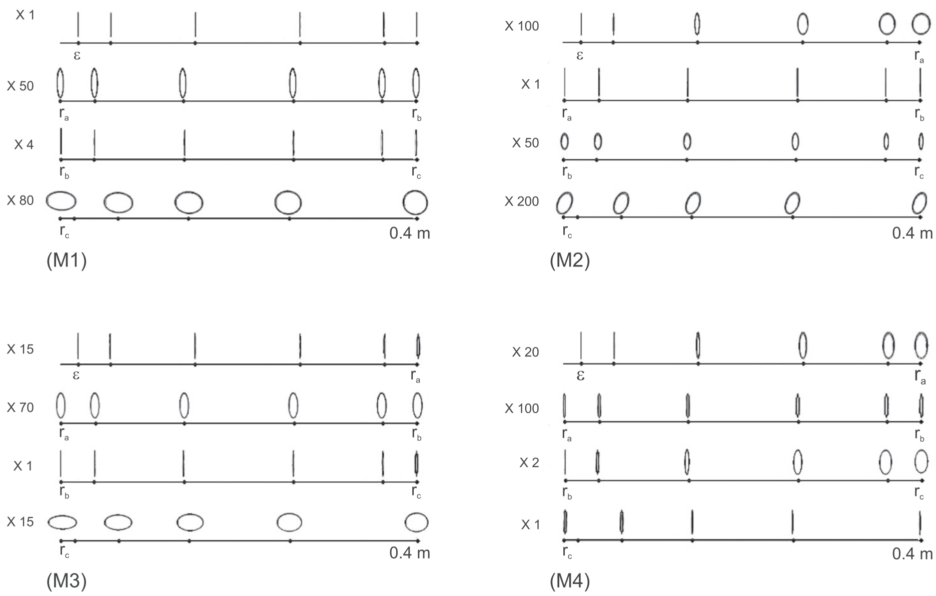

FIG. 13. Hard formation. Polarization of modes M1, M2, M3, and M4 in the inner mud, drill pipe, outer mud, and in the first 0.4 m of formation. For each mode, the particle orbits are plotted in the single domain with respect to the largest of the axial and radial particle velocities. The scaling factor is reported on the side.

axial and radial particle velocity more relevant in the formation domain.

B. Polarization

To analyze the relative magnitude of the axial and radial particle velocities, we calculate the orbits of modes M1, M2, M3, and M4 at three different frequencies, namely, 100, 300, and 600 Hz for the hard and soft formations using the properties shown in Table I (Fig. 12). The sign of the phase difference between the axial and radial particle velocities defines the direction of the orbits. Positive values corresponds to counterclockwise (+) and negative values to clockwise (–) orbits. The orbits of the four modes are calculated in the centre of the pipe and the fluid domains and at one and half the borehole radius in the formation. For each mode, the orbits are displayed with respect to the maximum of the axial and radial particle velocities.

In order to appreciate the relative variations of the axial and radial particle velocities along the radial direction, we calculate the particle orbits in different points of the inner fluid, drill pipe, outer fluid, and formation domains at the fixed frequency of 300 Hz. Figures 13 and 14 show the polarization of modes M1, M2, M3, and M4 plotted in each domain with respect to the largest of the axial and radial particle velocities, specifying the scaling factor, in the hard and soft formation, respectively.

Now we focus on the behaviour of the individual modes in each domain. Mode M1 [Figs. 12(a) and 12(b) for the hard and soft formation, respectively] is mainly localized in the inner fluid layer, with negligible radial particle velocity. Its orbits are positive in the fluid domains and negative in the solid domains. At the higher frequency of 600 Hz, the radial component of this mode can be seen in the soft formation [Fig. 12(b)]. The amplitudes of the radial and axial particle velocities of mode M1 observed in the inner mud are 50

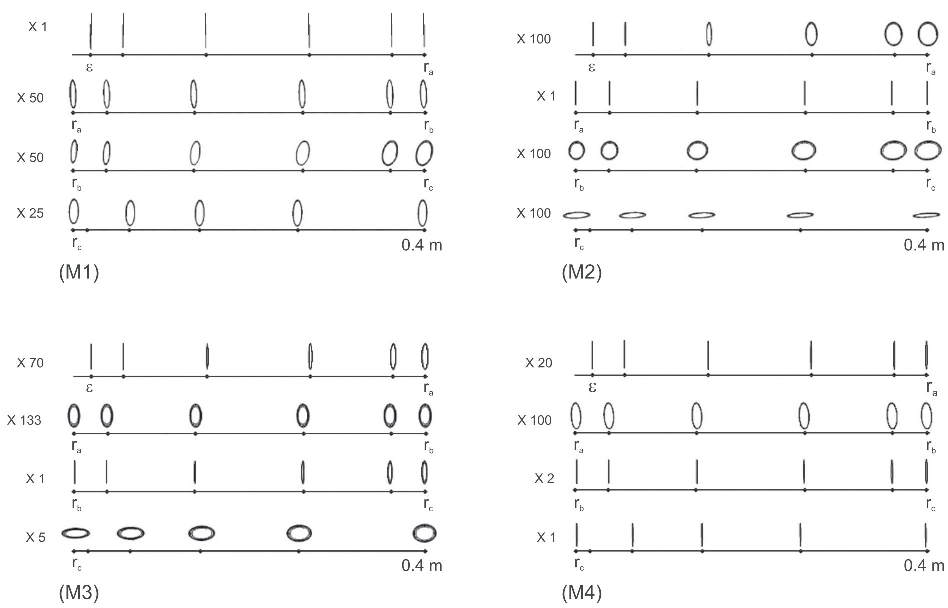

FIG. 14. Soft formation. Polarization of modes M1, M2, M3, and M4 in the inner mud, drill pipe, outer mud, and in the first 0.4 m of the formation. For each mode, the particle orbits are plotted in the single domain with respect to the largest of the axial and radial particle velocities. The scaling factor is reported on the side.

times higher than that in the drill pipe (Figs. 13 and 14). In the presence of hard formation, the energy of the radial and axial particle velocity components of mode M1 is mainly confined in the inner mud and partially in the outer mud, where the orbits are only four times weaker than that in the inner fluid and the radial motion still remains negligible. In the presence of the soft formation, the signal of mode M1 is better detectable in the formation, where the scale factor is 25 compared to 80 in the presence of hard formation.

The pipe mode M2 has a dominantly vertical orbit and it is felt mainly in the pipe [Figs. 12(c) and 12(d)]. The phase of the axial particle velocity is greater than that of the radial particle velocity in the outer fluid and in both the formations. The amplitudes of the radial and axial particle velocities recorded in the other domains are lower than that observed in the drill pipe but more energy is trapped in the outer fluid in the presence of hard formation (Figs. 13 and 14, M2).

Mode M3 has prevalently a vertical orbit in the outer fluid for both the hard [Fig. 12(e)] and soft [Fig. 12(f)] formations even though its radial component increases with frequency in the presence of the soft formation. The orbit directions are the same as those of the fluid mode M1, positive in the fluid domains and negative in the solid domains. Figures 13 and 14, M3, show that the radial particle velocity component increases approaching the formation, as expected for the so-called tube waves.[20] Like for the other modes the presence of hard formation limits the energy flow out of the outer mud/formation boundary.

The formation M4 mode has a dominantly vertical orbit for both the hard [Fig. 12(g)] and the soft [Fig. 12(h)] formations. The radial component begins to grow in the hard formation at the higher frequency 600 Hz. The magnitude of the orbits recorded in the formation and in the other domains are the same, both in the presence of hard (Fig. 13, M4) and soft (Fig. 14, M4) formations. Some differences can be observed in the relative magnitudes of the axial and particle velocities in the outer mud, where the radial component increases approaching the formation.

To further analyse the particle motion, we calculate the radial and axial displacements of mode M3 at given frequencies for the model proposed by Rama Rao and Vandiver[1] in the presence of soft formation and drill pipe (see Table III). Figure 15 shows the comparison between (a) the particle orbits of mode M3 calculated by Rama Rao and Vandiver[1] at 100, 300, and 1000 Hz and (b) that calculated with our numerical simulation at 100, 300, and 700 Hz using the rigid boundary condition at the borehole axis. The radial displacement component of mode M3 increases with frequency and

TABLE III. Material and geometrical properties. Soft formation with drill pipe (Ref. 1).

	v_P (m/s)	v_S (m/s)	ρ (g/cm^3)	ε (cm)	r_a (cm)	r_b (cm)	r_c (cm)	r_d (m)
Inner mud	1558	0	1.000	0.19	5.32	—	—	—
Drill pipe	5900	3400	7.800	—	5.32	6.35	—	—
Outer mud	1558	0	1.000	—	–	6.35	15.24	—
Soft formation	1409	813	2.000	—	–	–	15.24	100

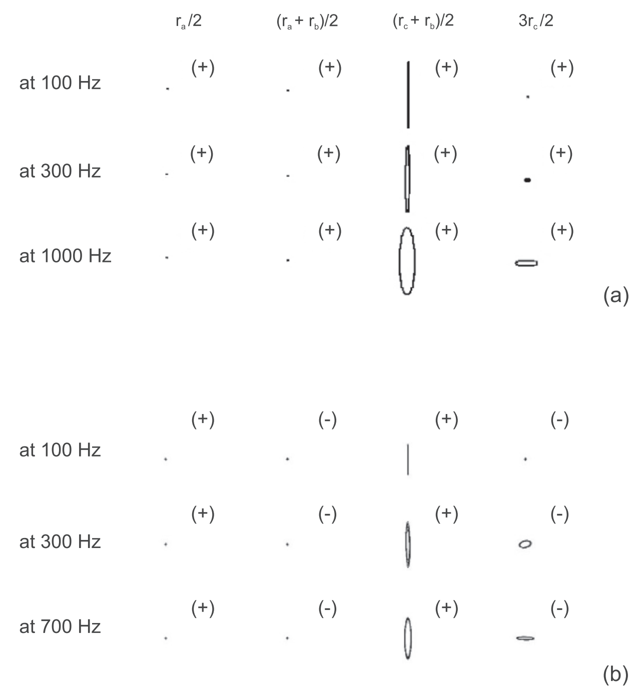

FIG. 15. Comparison between (a) the particle orbits of mode M3 modified after Rama Rao and Vandiver (Ref. 1) at 100, 300, and 1000 Hz and (b) that computed with the numerical simulation at 100, 300, and 700 Hz, using the rigid boundary condition at the borehole axis. The orbits directions are specified by (+) if counterclockwise and (–) if clockwise.

it is evident both in the analytical solution of Rama Rao and Vandiver[1] and in our numerical results. The direction of the orbits is counterclockwise corresponding to a positive phase difference (+) between the axial and radial displacement components in the two fluid domains, both in the analytical and numerical solutions. The orbit directions of mode M3 calculated with the numerical approach are clockwise (–) in the drill pipe and in the formation.

V. CONCLUSIONS

We analyse borehole wave-guide signals, using a full-wave numerical grid method, implemented in axis-symmetric multi-domains represented by polar coordinates. The systems consist of drill string and formation, including the inner and outer mud. The approach uses the rigid boundary condition to avoid the singularity in the inner-fluid domain at the origin. The results are validated by analytical solutions and the analysis of the mode amplitudes across the vertical cross-section of the cylindrical layers, together with the properties of the orbital particle motions at different locations. The vibration modes confirm the expected results for a relevant known in literature. The use of the rigid boundary condition prevents the inner fluid pressure to vanish. The analysis shows that the wave modes at the outer boundary of the borehole, at the formation contact, are influenced by the compressional-wave velocity and density of the formation.

Although other approaches, analytical and pseudo-spectral method provide dispersion relations for the characterization of downhole measurements, the elastic numerical approach presented in this work provides a powerful tool to investigate well acoustic data and formation radiation in arbitrary-geometry settings. The limitations of axis symmetry has to be overcome by development of full 3-D elastic codes.

[1]V. N. Rama Rao and J. K. Vandiver, "Acoustic of fluid-filled boreholes with pipe: Guided propagation and radiation," J. Acoust. Soc. Am. **105**, 3057–3066 (1999).

[2]J. M. Carcione and F. Poletto, "Simulation of stress waves in attenuating drill strings, including piezoelectric sources and sensors," J. Acoust. Soc. Am. **108**(1), 53–64 (2000).

[3]J. M. Carcione and F. Poletto, "Sound velocity of drilling mud saturated with reservoir gas," Geophysics **65**, 646–651 (2000).

[4]F. Poletto, J. M. Carcione, M. Lovo, and F. Miranda, "Acoustic velocity of SWD borehole guided waves," Geophysics **67**, 921–927 (2002).

[5]F. Poletto and F. Miranda, "Seismic while drilling: Fundamentals of drill-bit seismic for exploration," in *Handbook of Geophysical Exploration*, edited by K. Helbig and S. Treitel (Elsevier, New York, 2004), Vol. 35, pp. 1–520.

[6]A. Bakulin, A. Sidorov, B. Kashtan, and M. Jaaskelainen, "Real-time completion monitoring with acoustic waves," Geophysics **73**, E15–E33 (2008).

[7]H. Y. Lee, "Drillstring axial vibration and wave propagation in boreholes," Ph.D. thesis, Mass. Inst. Tech., Cambridge, MA, 1991.

[8]S. H. Lea and A. Kyllingstad, "Propagation of coupled pressure waves in borehole with drillstring," Society of Petroleum Engineers paper no. 37156 (1996).

[9]D. Kessler and D. Kosloff, "Acoustic wave propagation in 2-D cylindrical coordinates," Geophys. J. Int. **103**, 577–587 (1990).

[10]D. Kessler and D. Kosloff, "Elastic wave propagation using cylindrical coordinates," Geophysics **56**, 2080–2089 (1991).

[11]J. M. Carcione, F. Poletto, and B. Farina, "Simulation of axis-symmetric seismic waves in fluid filled boreholes in the presence of a drill string," Comput. Geosci. **12**, 593–604 (2008).

[12]J. M. Carcione, "Wave fields in real media: Wave propagation in anisotropic, anelastic, porous and electromagnetic media," in *Handbook of Geophysical Exploration*, 3rd ed., revised and extended, edited by K. Helbig and S. Treitel (Elsevier, New York, 2014), Vol. 38, pp. 1–515.

[13]V. N. Rama Rao, "The radiation and vibration of drilling tubulars in fluid-filled boreholes," Ph.D. thesis, Mass. Inst. Tech., Cambridge, MA, 1996.

[14]M. Malusa, J. M. Carcione, and F. Poletto, "Coupled axial waves in drill strings," in *67th EAGE Conference and Exhibition*, extended abstracts (2005), pp. 267, 2955–2958.

[15]F. Karpfinger, H. P. Valero, B. Gurevich, A. Bakulin, and B. Sinha, "Spectral-method algorithm for modeling dispersion of acoustic modes in elastic cylindrical structures," Geophysics **75**, H19–H27 (2010).

[16]J. M. Carcione, "Domain decomposition for wave propagation problems," J. Sci. Comput. **6**, 453–472 (1991).

[17]J. M. Carcione, "Modeling elastic waves in the presence of a borehole and free surface," in *64th Ann. Int. Mtg. SEG*, expanded abstracts (1994), pp. 747–750.

[18]D. Gottlieb and S. Orzag, "Numerical analysis of spectral methods, theory and applications," in *CBMS-NFS Regional Conference Series in Applied Mathematics* (SIAM, Philadelphia, PA, 1977), Vol. 26, pp. 1–170.

[19]J. M. Carcione and F. Poletto, "Synthetic logs of multipole sources in boreholes based on Kelvin–Voigt stress-strain relation," Geophys. J. Int. **174**, 808–814 (2008).

[20]C. H. Cheng and M. N. Toksöz, "Generation, propagation and analysis of tube waves in a borehole," in *Vertical Seismic Profiling, Part B: Advanced Concepts*, edited by M. N. Toksöz and R. R. Stewart (Geophysical Press, London, 1984), pp. 276–287.